2020 EAGE ANNUAL
82ND CONFERENCE + EXHIBITION
AMSTERDAM | THE NETHERLANDS
NOW IN WINTER
8-11 DECEMBER

We_P03_08A

Full Waveform Inversion Using Wave Equation Reflectivity Modeling

Y. Yang[1]*, J. Ramos-Martinez[1], D. Whitmore[1], A. Valenciano[1], N. Chemingui[1]

[1] PGS

Summary

Full Waveform Inversion (FWI) is routinely used to improve the accuracy and resolution of velocity models. However, utilizing reflections to produce low-wavenumber updates creates more operational challenges than using transmitted events. In order to simulate backscattered sensitivity kernels, FWI needs hard boundaries in the velocity/density models. Alternatively, one can apply the wave equation and first-order Born approximation to decompose the seismic wavefields into background and perturbation. Here, we derive an acoustic wave equation in terms of vector reflectivity to be used as the wave's propagation engine of FWI. The new derivation results from the change of variables from impedance to reflectivity in the variable density wave equation. The main advantages of its insertion in our FWI algorithm are the following: it does not require the construction of density/hard boundaries in the velocity model to generate reflections; it allows the use of reflected events without the need of solving two different wave equations in the forward and backward propagation; it is more accurate than the method based on the first-order Born approximation to perturbation theory. We show synthetic and field data examples illustrating the advantages of the new algorithm.

Introduction

Full Waveform Inversion (FWI) with transmitted events is a robust technology used to improve the resolution of the velocity models. However, using transmitted events only provides velocity updates for the maximum penetration depth of the recorded diving and head waves, which depends on the maximum offset in the data. The use of reflected waves overcomes this limitation (e.g., Xu et al., 2012; Zhou et. al., 2015). Nevertheless, using reflections can create operational challenges for FWI algorithms. The conventional cross-correlation gradient will contain the low-wavenumber tomography term (rabbit-ears) as well as the high-wavenumber migration term (migration isochrones). As the migration term is usually one order of magnitude larger in amplitude than the tomography term, the high-wavenumber components of the velocity field are updated faster than low wavenumber components. In other words, the solution converges to a local minimum with the wrong low-wavenumber components (Mora, 1989). Therefore, removing the strong isochrones to update the model low-wavenumber components first is one of the key components for a robust reflection-based FWI.

Different strategies have been proposed to separate the low- from the high-wavenumber components of the velocity updates. The most common approach used is based on separating the wavenumber features from the velocity field (Xu et al., 2012). This method requires the solution of two different acoustic wave equations. First, resolve the conventional wave equation to generate the events corresponding to the smooth background velocity field. Following this, solve a linearized version of the wave equation resulting from applying the Born approximation, to simulate the scattered events corresponding to the high-wavenumbers. Other strategies perform the separation directly on the gradient. For example, Gomes and Chazalnoel (2016) use the up- and down-wavefield separation. However, this approach is not able to remove the isochrones produced by horizontal wave propagation as the Hilbert transform is only applied in the vertical direction, which leads to "migration leakage". Scattering angle filtering (Alkhalifah, 2014) is another way to separate the gradient wavenumber components but it increases the computational cost of the inversion. Ramos-Martinez et al. (2016) proposed a robust and efficient gradient that removes the isochrones and produces clean low-wavenumber updates.

In this paper, we propose a new efficient FWI workflow for transmissions and reflections based on a novel acoustic wave equation that uses velocity and reflectivity as parameters (Whitmore et al., 2020). The new modeling engine does not require the construction of a density model to simulate the scattered events, and provides the full forward and backward wavefield in one modeling realization. The separation of low- and high-wavenumber components in the gradient is performed using an efficient implementation of the impedance and velocity sensitivity kernels (Ramos-Martinez et al., 2016). First, we show the derivation of the new wave equation in terms of velocity and reflectivity and its combination with the method to separate the wavenumber components. Then, we illustrate the performance of the proposed workflow in synthetic and field data examples.

Method

The variable density acoustic wave equation is written as:

$$\frac{1}{V(\boldsymbol{x})^2}\frac{\partial^2 P(\boldsymbol{x},t)}{\partial t^2} - \rho(\boldsymbol{x})\nabla\cdot\left(\frac{1}{\rho(\boldsymbol{x})}\nabla P(\boldsymbol{x},t)\right) = S(\boldsymbol{x},t), \qquad (1)$$

where P is the complete pressure wavefield which is function of space $(\boldsymbol{x})$ and time (t), V is the velocity, ρ is the density and S is the source. From the definition of acoustic impedance ($Z(\boldsymbol{x})=\rho(\boldsymbol{x})V(\boldsymbol{x})$), and doing a change of variable from impedance to reflectivity, equation (1) can be written as:

$$\frac{1}{V(\boldsymbol{x})^2}\frac{\partial^2 P(\boldsymbol{x},t)}{\partial t^2} - \nabla^2 P(\boldsymbol{x},t) - \frac{\nabla V(\boldsymbol{x})}{V(\boldsymbol{x})}\cdot\nabla P(\boldsymbol{x},t) + 2\boldsymbol{R}(\boldsymbol{x})\cdot\nabla P(\boldsymbol{x},t) = S(\boldsymbol{x},t). \qquad (2)$$

Here, $\boldsymbol{R}(\boldsymbol{x}) = \frac{1}{2}\frac{\nabla Z(\boldsymbol{x})}{Z(\boldsymbol{x})}$ is the vector reflectivity (Sheriff and Geldart, 1995), which can be derived from migration. Notice that for a smooth velocity model, the third term in equation (2) can be neglected and the scattering is mainly produced by the reflectivity term. For constant density, the last two terms on the left-hand side are zero and the equation has the same form of the scalar wave equation. Compared with Born modeling (Mora, 1989), no approximation is done. The modeling is accurate under any situation.

Also, only one wave equation needs to be solved comparing with two equations needed in Born modeling.

To separate the low- (tomography term) from the high-wavenumber (migration term) components in the gradient, we use an efficient implementation of the impedance (Whitmore and Crawley, 2012) and the velocity (Ramos-Martinez et al., 2016) sensitivity kernels. The velocity kernel is defined as

$$K_V(\boldsymbol{x}) = \frac{1}{2I(\boldsymbol{x})}\left[\int \left(W_1(\boldsymbol{x},t)\frac{1}{V(\boldsymbol{x},t)^2}\frac{\partial P(\boldsymbol{x},t)}{\partial t}\frac{\partial Q(\boldsymbol{x},t)}{\partial t} - W_2(\boldsymbol{x},t)\nabla P(\boldsymbol{x},t)\cdot\nabla Q(\boldsymbol{x},t)\right)dt\right], \quad (3)$$

where W_1, W_2 are dynamic weights, P and Q are forward and adjoint wavefields and I is the illumination term.

Synthetic examples

First, we compute the sensitivity kernel for a homogeneous layer overlaying a half-space from the proposed approach and compare it with that computed from the Born approximation. Figure 1 shows the results for both cases. As observed, the new workflow produces rabbit ears with less artifacts near the reflector.

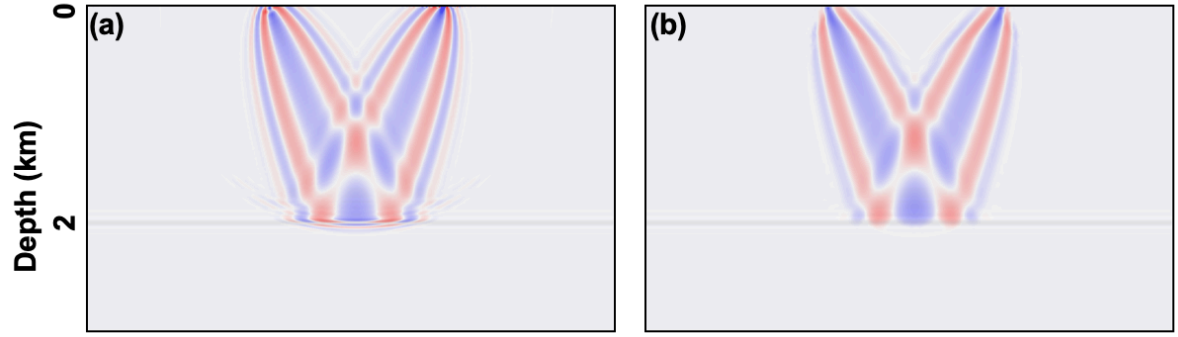

Figure 1 *Rabbit ears from (a) Born modeling and from (b) the new reflectivity modeling engine and velocity sensitivity kernel. Background shows the migrated image used as input reflectivity in the modeling.*

Next, we compare the different inversion strategies by using a modified 2D slice of the SEG Overthrust model that includes a water layer. We use a fixed-spread acquisition geometry consisting of 81 shots and 601 receivers that are evenly distributed at a constant depth of 10 m. The data contained no offsets beyond 4 km. The initial model was a heavily smoothed version of the true model. The initial reflectivity model was generated from reverse time migration using the Inverse Scattering Imaging Condition (Whitmore and Crawley, 2012).

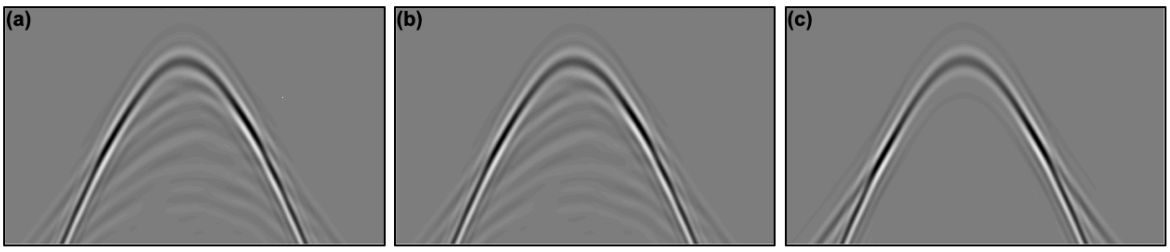

Figure 2 *(a) Synthetic shot gathers for the modified Overthrust model using velocity and density with variable density equation. (b) Modeling results using the new wave equation and the true reflectivity. (c) Velocity only modeling with the initial velocity model.*

Figure 2 shows the synthetic shot gathers that illustrate the performance of the new reflectivity modeling engine. The frequency bandwidth for the modeling ranged from 3 Hz to 7.5 Hz. From the true reflectivity and velocity, our reflectivity modeling method gives the same seismic response as the modeling with the velocity and density. If only velocity is used in the modeling, the reflections are not

modeled (Figure 2c). Thus, the reflectivity modeling engine provides a way to generate corresponding reflections by using the high-wavenumber reflectivity. The discrepancies between the modeling and the filed data can be used as targets to update model low-wavenumber in FWI.

The inversion results are shown in Figure 3. The maximum frequency used is 7.5 Hz. We muted all the diving waves and head waves so the inversion used only reflections. The new FWI improves the low-wavenumber contents of the velocity field (Figure 3c). This model is then used as the input of a conventional inversion (cross correlation gradient) to incorporated the high-wavenumber features of the model (Figure 3e). For comparison, we performed the inversion using FWI with a cross correlation gradient from the staring (smooth) velocity model (Figure 3d). As observed, the background model is better defined and high-wavenumber features are enhanced with our cascaded FWI workflow.

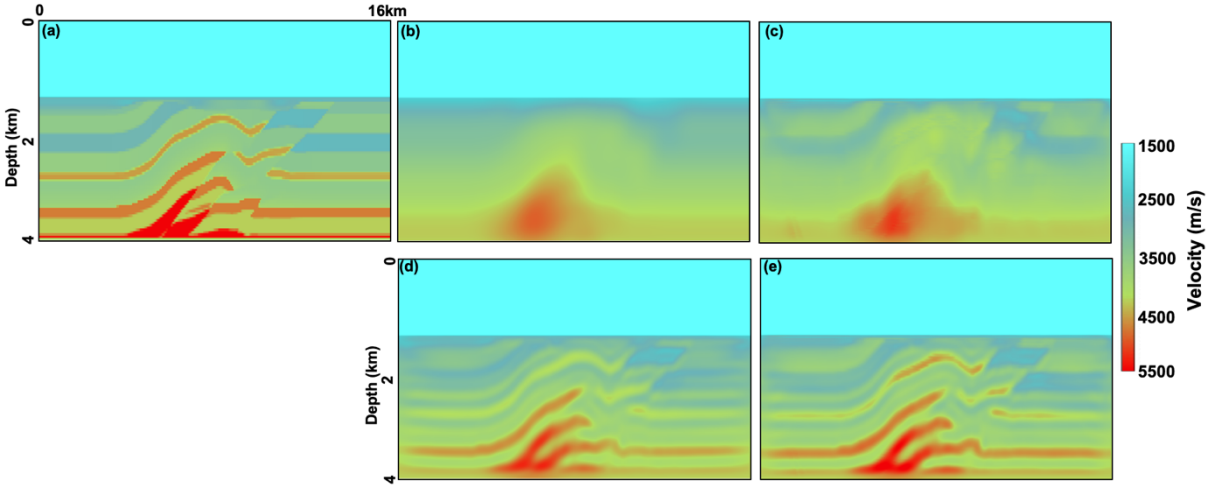

Figure 3 *Synthetic example for a modified version of the Overthrust model. (a) True velocity model. (b) Initial velocity model. (c) our FWI model using reflections. (d) FWI model using cross correlation gradient with (b) as the initial. (e) FWI model using cross correlation with (c) as the initial.*

Field data example

Finally, we applied the new FWI to a field data set acquired in the Canadian Orphan Basin. The geological setting is a challenging environment for Velocity Model Building (VMB). The data were acquired with dual-sensor streamers with offsets up to 8 km. The shallow part of the initial model was built using mostly transmitted waves in FWI (Frugier et. al., 2020). However, the water depths of approximately 2 km combined with 8km maximum offset makes it difficult to use FWI to update the model for depths beyond 4 km.

To update the velocity model deeper than the penetration of the diving wave, we applied our new FWI using only reflections. The data maximum frequency used in the inversion was 8Hz. We muted all the shallow reflections, the diving waves, and the multiples. The new FWI results show low-wavenumber updates deeper than 4km (Figure 4a). The reflectivity modeling, after the deep updates with FWI, shows better kinematic match for the deep reflections (Figures 4b and 4c). To further evaluate the model derived from FWI with reflections, we computed common image gathers. There, we observed that the new FWI velocity model improved the flatness of the offset gathers (see Figures 4d and 4e). On top of the low-wavenumber updates we performed FWI with a cross correlation gradient. The result of the cascaded FWI workflow matches the well log data (Figure 4f).

Conclusions

We have introduced an FWI workflow based on a modified acoustic wave equation that uses velocity and reflectivity as parameters. This provides an accurate way to simulate reflections that are used in the inversion, without the need to build a density model or use first-order Born approximation to decompose

the seismic wavefields. The new modeling engine is efficient as it computes the full acoustic wavefield in one modeling realization. The new FWI produces good results using synthetics and field data.

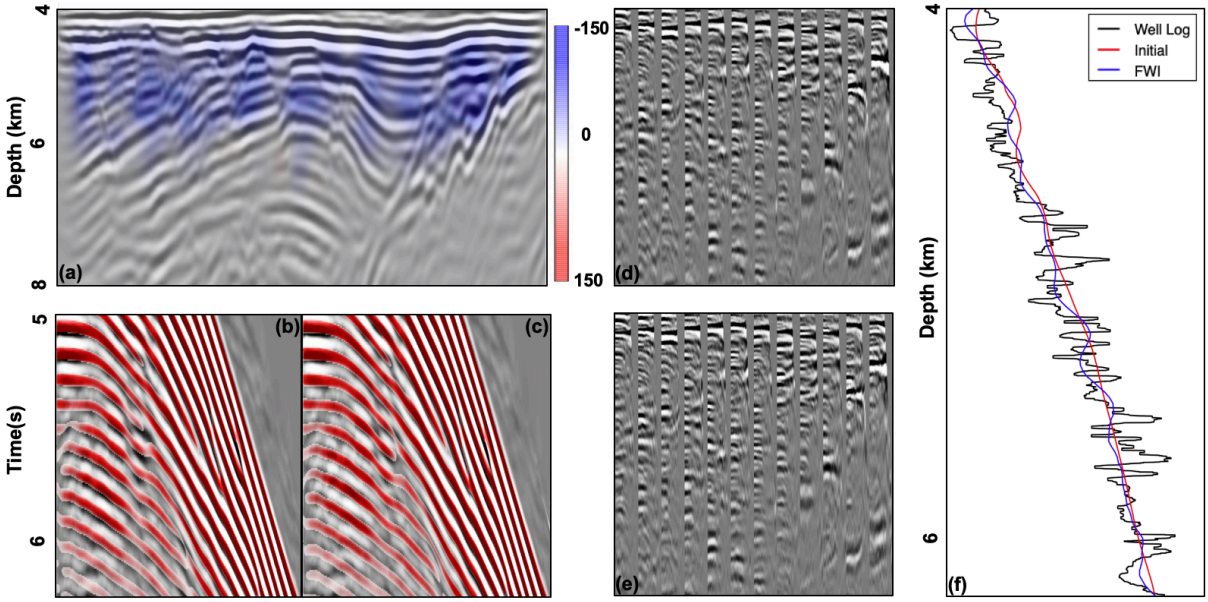

Figure 4 *(a) Velocity updates along with the final reflectivity. Comparison between reflectivity modeling results (red) and the real data (black) for (b) the initial model and (c) the FWI model. Migration gathers with (d) the initial model and (e) the FWI model. (f) Well log data (black) along with the initial (red) and the final FWI model (blue). Note the change in background and new details brought by the cascaded FWI workflow.*

Acknowledgements

We thank Tiago Alcantara and Mikhail Orlovich for their assistance in the field data example. We also thank PGS multiclient for their permission to publish the field data results.

References

Alkhalifah, T. [2014] Scattering-angle based filtering of the waveform inversion gradients, Geophysical Journal International, **200**(1), 363-373.
Frugier, E., Alcantara, T. and Virlouvet, B. [2020] High-resolution FWI model building using raw Geostreamer data: A case study in the Orphan basin deep waters, Geoconvention, in preparation.
Gomes, A., and N. Chazalnoel [2017] Extending the reach of FWI with reflection data: Potential and challenges, 87th Annual International Meeting, SEG, Expanded Abstracts, 1454-1459.
Mora, P. [1989] Inversion= migration+ tomography, Geophysics, **54**(12): 1575-1586.
Ramos-Martinez, J., S. Crawley, K. Zou, A. A. Valenciano, L. Qiu and N. Chemingui [2016] A robust gradient for long wavelength FWI updates, 78th EAGE Conference & Exhibition, Extended Abstracts.
Sheriff, R. E. and L. P., Geldart. [1995] Exploration Seismology, Cambridge University Press, 2nd Edition.
Tarantola, A. [1984] Inversion of seismic reflection data in the acoustic approximation: Geophysics, **49**, 1259–1266.
Whitmore, N. D. and S. Crawley [2012] Application of RTM inverse scattering imaging conditions, 82nd Annual International Meeting, SEG Expanded Abstracts.
Whitmore, D., J. Ramos-Martinez, Y. Yang and A. A. Valenciano [2020] Full wavefield modeling with vector reflectivity, 82nd EAGE Conference & Exhibition, Extended Abstracts, submitted.
Xu, S., Wang, D., Chen, F., Zhang, Y. and Lambaré, G. [2012] Full waveform inversion for reflected seismic data, 74th EAGE Conference & Exhibition, Extended Abstracts, W024.
Zhou, W., R. Brossier, S. Operto, and J. Virieux [2015] Full waveform inversion of diving & reflected waves for velocity model building with impedance inversion based on scale separation: Geophysical Journal International, **202**, 1535–1554.